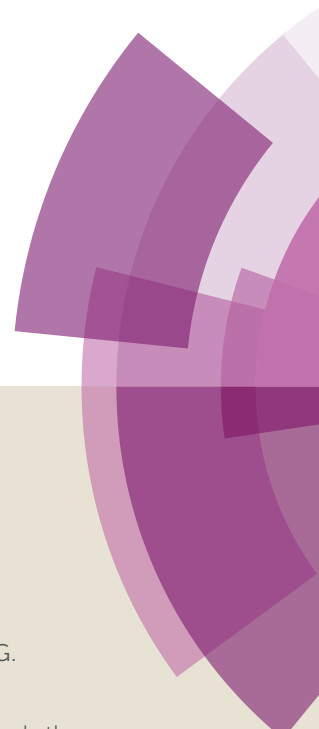


# Journal of Materials Chemistry C

Accepted Manuscript



This article can be cited before page numbers have been issued, to do this please use: I. PIBIRI, A. Beneduci, M. Carraro, V. Causin, G. Casella, G. A. Corrente, G. Chidichimo, A. Riccobono, A. Pace and G. Saielli, *J. Mater. Chem. C*, 2019, DOI: 10.1039/C9TC01697J.



This is an Accepted Manuscript, which has been through the Royal Society of Chemistry peer review process and has been accepted for publication.

Accepted Manuscripts are published online shortly after acceptance, before technical editing, formatting and proof reading. Using this free service, authors can make their results available to the community, in citable form, before we publish the edited article. We will replace this Accepted Manuscript with the edited and formatted Advance Article as soon as it is available.

You can find more information about Accepted Manuscripts in the [author guidelines](#).

Please note that technical editing may introduce minor changes to the text and/or graphics, which may alter content. The journal's standard [Terms & Conditions](#) and the ethical guidelines, outlined in our [author and reviewer resource centre](#), still apply. In no event shall the Royal Society of Chemistry be held responsible for any errors or omissions in this Accepted Manuscript or any consequences arising from the use of any information it contains.

## Mesomorphic and electrooptical properties of viologens based on non-symmetric alkyl/polyfluoroalkyl functionalization and on oxadiazolyl-extended bent core

Received 00th January 20xx,  
Accepted 00th January 20xx

DOI: 10.1039/x0xx00000x

www.rsc.org/

Ivana Pibirj,<sup>a\*</sup> Amerigo Beneduci,<sup>b,\*</sup> Mauro Carraro,<sup>c</sup> Valerio Causin,<sup>c</sup> Girolamo Casella,<sup>c,d</sup> Giuseppe Chidichimo,<sup>b</sup> Giuseppina Anna Corrente,<sup>b</sup> Andrea Pace,<sup>a</sup> Alessio Riccobono,<sup>a</sup> and Giacomo Saielli<sup>e,\*</sup>

Two different sets of ionic liquid crystals based on bistriflimide salts of non-symmetrically substituted polyfluorinated bipyridinium (viologens) and bent symmetrically substituted dialkyl-oxadiazolyl-bipyridinium have been synthesized, in order to study the effect, on the mesomorphic and electrooptical properties, of the non symmetric functionalization (alkyl chain and fluoroalkyl chains of different length) on the two pyridinium rings and additionally the effect of a bent conjugated spacer among the two pyridinium units of the viologen. POM and DSC characterization show that the synthesized salts have a mesomorphic and, in some cases, polymesomorphic behaviour in a wide thermal range, also encompassing room temperature. Some of the compounds exhibit SmA phase in addition to more ordered smectic phases at lower temperature. The presence of a fluorinated chain on one side seems to generally increase the stability of the ionic liquid crystal SmA phase compared to alkylated analogues of viologens. Moreover, the insertion of the bent oxadiazolyl spacer between the two pyridinium units, has a significant effect on the mesophase behaviour leading to dendritic textures recalling those of banana phases. Electrochemical characterization by cyclic voltammetry shows that the presence of a fluorinated moiety causes an easier reduction compared to typical alkyl viologens while the oxadiazolyl-bipyridinium derivatives have more negative reduction potentials. Spectroelectrochemical experiments show that differently to the classic viologens showing the typical electrochromic band of their radical cation, the oxadiazolyl insertion between the two pyridinium moieties hampers electrochromism due to a resonance coupling missing between the N redox centers. Interestingly, electrochromism of the polyfluorinated viologens, besides being observed in solution is still observed in the ionic liquid crystal smectic phase of some of the salts of this series, upon radical cation formation; additionally the spectrum exhibits a further electrochromic band in the near infrared range which is not observed in solution.

### Introduction

Among organic materials, alkylated viologens have been the subject of several studies concerning their structural properties,<sup>1</sup> mesomorphism,<sup>2–7</sup> self-assembly<sup>8</sup> and the formation of mesoporous hybrid materials.<sup>9</sup> Moreover their optoelectronic properties,<sup>10</sup> their use as oxidation catalysts for

alkaline carbohydrate fuel cells,<sup>11</sup> as well as ionic liquid electrolytes in electrochromic devices,<sup>12–14</sup> have been also widely investigated. In this context, also the synthesis of symmetrically substituted polyfluoroalkyl viologens has been reported.<sup>15</sup>

In all the cases mentioned above, the electronic and redox properties depend on the particular conjugated structure of the  $\pi$  system of the two pyridinium units, while the aggregation behaviour of the material/compound is dictated by the dual nature of the molecule:<sup>16</sup> an ionic rigid core linked to flexible hydrophobic alkyl/fluoroalkyl chains.

In particular, the mesomorphism of viologen-based ionic liquid crystals (ILCs) has been widely investigated (for an extensive review concerning ILCs see Ref.<sup>17</sup>). Symmetric viologens,<sup>6,18</sup> as well as polymers,<sup>19–21</sup> have been studied by Bhowmik and co-workers. Some of us investigated non-symmetrically substituted viologens (with different length alkyl chains)<sup>5</sup> as well as the effect of the increased steric hindrance of the viologen core.<sup>22</sup> Together with the more common ionic smectic phases also cubic phases<sup>23</sup> and columnar phases<sup>24</sup> based on

<sup>a</sup> Dipartimento di Scienze e Tecnologie Biologiche, Chimiche e Farmaceutiche (STEBICEF), Università degli Studi di Palermo, Viale delle Scienze Ed. 17, 90128, Palermo, Italy. \*Email: ivana.pibirj@unipa.it

<sup>b</sup> Department of Chemistry and Chemical Technologies, University of Calabria, Via P. Bucci, Cubo 15D, 87036 Arcavacata di Rende (CS), Italy. \*Email: amerigo.beneduci@unical.it

<sup>c</sup> Department of Chemical Sciences (DISC), University of Padova, Via Marzolo, 1 – 35131, Padova, Italy.

<sup>d</sup> Dipartimento di Scienze della Terra e del Mare, Università degli Studi di Palermo, Via Archirafi, 22, 90123 Palermo, Italy

<sup>e</sup> Istituto CNR per la Tecnologia delle Membrane, Sede Secondaria di Padova, Via Marzolo, 1 – 35131, Padova, Italy. \*Email: giacomo.saielli@unipd.it

Electronic Supplementary Information (ESI) available: [details of any supplementary information available should be included here]. See DOI: 10.1039/x0xx00000x

viologens have been reported. Interestingly, viologens systems, having a rigid and di-cationic core, exhibit a LC phase with relatively large and hydrophobic anions, such as  $[\text{PF}_6]^-$  and  $[\text{Tf}_2\text{N}]^-$  and crystalline phase with halides; this is somewhat at variance with the behaviour of imidazolium salts, where LC phases of halides are quite common for chains larger than about 12 carbon atoms, while with the large bistriflimide anion the isotropic liquid phase is stabilized and no mesophase is found except for a chain length of at least 22 carbon atoms.<sup>25</sup> The effect of the anion on the mesophase behaviour of diphenylviologens has been also investigated by Lai and co-workers.<sup>26</sup>

Mesomorphic, electrochemical as well as electrooptical properties of viologens can be significantly affected by the extension of the conjugated structure, through the insertion of different groups between the pyridinium units. To date, the only LC extended viologens reported in the literature are the symmetric thienoviologens.<sup>27</sup> They show a range of mesophases spanning the nematic/discotic columnar,<sup>28</sup> rectangular columnar<sup>27</sup> and smectic ones.<sup>29</sup> Such a polymesomorphism can be tuned by the length of the alkyl chains and by the type of anion.<sup>28</sup> The mesophase nanosegregation in these ILCs leads to the formation of ionic and electronic conductive pathways which are necessary to achieve the intriguing electrofluorescence and electrochromic properties in the bulk.<sup>29–32</sup>

The choice of the conjugated core is crucial for tailoring viologens with specific bulk properties. Of particular interest is the investigation of the effects of a bent aromatic core on the mesomorphism and electrochemistry/electrooptic of extended viologens. To this aim, the 1,2,4-oxadiazole moiety constitutes a good choice as a bent heterocyclic spacer.<sup>33</sup> 1,2,4-oxadiazoles are promising compounds for their applications in materials<sup>34–40</sup> besides their well-known application in pharmaceutical science.<sup>41–47</sup> The peculiar angle between the substituents on C(3) and C(5) of 1,2,4-oxadiazole has been considered as responsible for a better molecular organization in the liquid crystals mesophase.<sup>48–52</sup>

In particular, concerning 1,2,4-oxadiazolyl-methylpyridinium salts, we previously reported the synthesis<sup>53</sup> and the thermotropic behaviour.<sup>40</sup> The same core oxadiazolyl-methylpyridinium linked to long alkyl chain showed a further shift in the melting points, in fact alkyl-1,2,4-oxadiazolyl-methylpyridinium salts were room temperature ILCs.<sup>54</sup> Bis (4-pyridyl)oxadiazoles have been exploited as organic bases in order to realize a set of Protic Ionic Liquids (PILs)<sup>34</sup> and as tectons for the preparation of a library of X-bonded supramolecular adducts with defined geometry.<sup>35</sup>

Very interesting results have been reported for a set of 1-alkyl-3-poly-fluoroalkyl imidazolium iodide, as fluorinated ionic liquids crystals (FILCs) showing a SmA phase, to be exploited as redox electrolyte in solar cells and other electronic devices.<sup>55</sup> Moreover, novel triazolium ionic liquids and ionic liquid crystals bearing both perfluorocarbon and hydrocarbon moieties have been recently reported,<sup>56</sup> for this class of salts the phase behaviour and physical properties are tunable as a function of chain length and fluorine content: shorter perfluoroalkyl chains

( $\text{C}_3\text{F}_7$ ) do not promote mesogenic behaviour, even when associated to long  $\text{C}_{14}\text{H}_{29}$  alkyl chain; longer  $\text{C}_{17}\text{H}_{35}$  chains induce SmA phases. These salts have shown high ion mobility and conductivity increasing exponentially with temperature, being higher for isotropic liquid phases when compared to the SmA phases.<sup>56</sup>

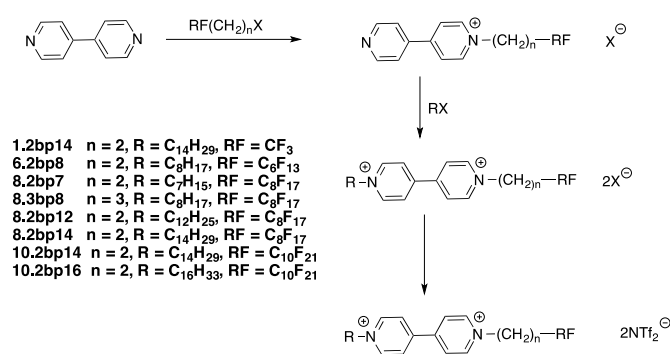
In this study we have selected two sets of compounds (see Scheme 1 and Scheme 2), depicted as **bp** and **obp** series. The first set (**bp** series) are non-symmetric 4-4'-bipyridinium salts of bistriflimide (NTf<sub>2</sub>) with an alkyl chain on one side and a polyfluorinated chain on the other side. The reason of this choice is to study the effect of the insertion of a fluorinated component just on one side of the viologen salts, to stress the phase segregation between the alkyl and polyfluoroalkyl chains linked to the bipyridinium core.

The second set of compounds investigated (**obp** series), polyfluoroalkyl-bis (4-pyridinium)oxadiazole bistriflimide salts, has been selected willing to prepare a set of bent scaffolds, to compare to the linear scaffold of viologen compounds, in order to study the different molecular organization in the mesophase. In fact, the 1,2,4-oxadiazole heterocyclic spacer allow us to access to bent structures with bending angles between the attached pyridines of approximately 140°. The main focus of the paper, besides the characterization of the thermal behaviour, is also the investigation of the performance of the materials in electrooptic devices.

## Results and Discussion

### Synthetic procedures.

The synthesis of the set of viologens has been carried out in two steps (see Scheme 1), as the higher reactivity of alkylating reagents should give rise, also in defect of alkylated agent, to bisalkylated products, we preferred to perform the polyfluoroalkylation as first step, in order to obtain just the monopolyfluoroalkyl derivative.

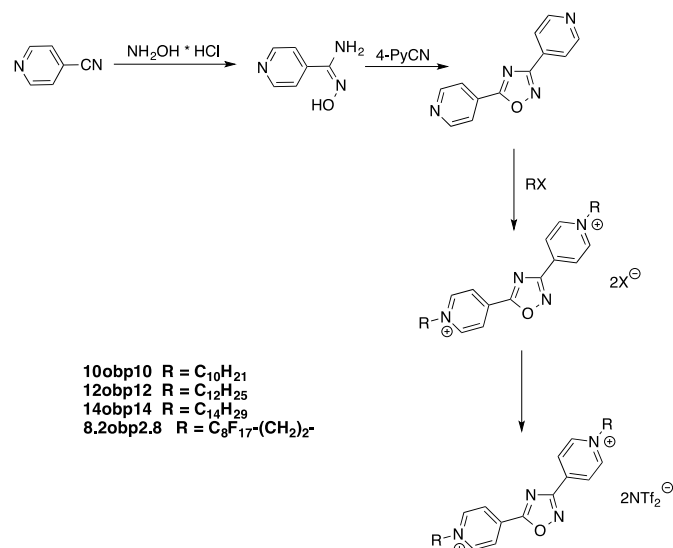


**Scheme 1.** Compounds containing a bipyridinium core (**bp**), will be labelled as **M.NbpL** where **M** represents the number of fluorocarbons on the polyfluorinated chain, **N** is the number of carbons of the aliphatic bridge linked to the Nitrogen of the pyridinium moiety and **L** is the number of carbons in the alkyl chain. Compounds studied here are the bistriflimide (NTf<sub>2</sub>) salts.

The monopolyfluoroalkyl derivative was further reacted with alkyl iodide/bromide in order to obtain the asymmetrically substituted viologen.

The alkylation/polyfluoroalkylation steps have been performed in two ways: a thermal reaction lasting 4-7 days with slightly higher yields and a microwave reaction with lower yields but lasting just 3-5 hours.

The so obtained bis iodide/bromide was converted to bistriflimide salt by anion metathesis reaction allowing to obtain the **bp** salts series.



**Scheme 2.** Oxadiazolylbipyridinium will be labelled as **LobpL** and **M.NobpN.M**, where M represents the number of fluorocarbons on the polyfluorinated chain, N is the number of carbons of the aliphatic bridge linked to the Nitrogen of the pyridinium moiety and L is the number of carbons in the alkyl chain. Compounds studied here are the bistriflimide (NTf<sub>2</sub><sup>-</sup>) salts.

Oxadiazolylbipyridine were prepared as reported<sup>34</sup> (see Scheme 2), the bis-alkylation/bis-polyfluoroalkylation step has been performed and the following anion metathesis allowed to obtain the salts of the **obp** series.

All precursor salts, usually bromides and iodides, did not show any mesophase nor a low-melting liquid phase, therefore they have not been considered further in this work. In contrast,

because of the well-known depressing effect of the NTf<sub>2</sub><sup>-</sup> anion on the melting point of quaternary nitrogen salts, the bistriflimide derivatives prepared by anion metathesis showed interesting properties, as they exhibited mesomorphism in a range of temperature feasible for potential applications in real devices. Further details of the synthetic procedures and characterization of the compounds can be found in ESI.

### Thermal behaviour

The thermal behaviour and phase sequence of the compounds have been investigated by Polarized Optical Microscopy (POM) and Differential Scanning Calorimetry (DSC). Figure 1 shows some characteristic textures observed through the POM micrographs for some selected compounds, while the rest of the POM Figures are included in Supporting Information together with the DSC curves. Thermal data, obtained during the cooling run of the DSC, and compiled in Table 1. We have not investigated in detail the Cr-Cr transitions between different crystal polymorphs that can be observed in some DSC traces, since they were not relevant for the behaviour and application of the materials.

**1.2bp14** has a low melting point into the isotropic liquid, well below 100 °C so that it can be considered an ionic liquid. The clearing temperature observed at POM on cooling from the Iso state is 63 °C. In the DSC trace, the clearing transition can be detected only in the heating scan and corresponds to the peak above 60 °C. The transition at 44.8 °C found in the thermogram on cooling, is instead attributed to a SmX-Cr transition, according to its relatively large value of ΔH. The Iso-SmX transition is clearly detected at POM by the formation of a marble texture (Figure 1a and S1 and S2 in ESI). Comparison of the thermal behaviour of **1.2bp14** with the non-fluorinated analogue **2bp14** described in the literature<sup>3</sup> shows that addition of a CF<sub>3</sub> group induces phase segregation besides decreasing slightly the melting temperature. Increasing the length of the fluorine moiety, we observe for **6.2bp8** that the isotropic liquid phase range is shifted to higher temperatures.



**Figure 1.** POM microphotographs obtained on cooling from the isotropic liquid. a) marble texture of **1.2bp14** at 53 °C; b) mosaic textures of **8.2bp7** at 92 °C; c) mosaic texture of **8.3bp8** at 165 °C; d) fan shaped texture of **8.2bp12** at 120 °C; e) fan shaped textures of **10.2bp16** at 190 °C; f) fan shaped textures of **10obp10** at 150 °C. g) dendritic textures of **12obp12** at 45 °C. h) dendritic textures of **14obp14** at 196 °C. The white&blue bars correspond to 100 μm.

On cooling, (5 °C/min) a transition is observed at the microscope at 155 °C characterized by a marble texture, which corresponds to the peak at 158.7 °C in the DSC trace (Figure S3). On further cooling, at 115 °C a change in the birefringence of the marble texture was detected (Fig. S4). Finally, below 52 °C a significant texture change involving a large  $\Delta H$  value occurs (Table 1 and Figure S4), indicating sample crystallization.

By a further increase of 2 carbons of the fluorinated moiety and a decrease of the alkylated one, in **8.2bp7** we observe a mosaic texture (Figure 1c and Figure S6 of ESI), on cooling from the melt, that suggests an ordered smectic phase between the isotropic and crystal phase, with shorter mesophase range. For this compound the clearing point was better assessed by inspection of the behaviour under the microscope, see ESI (Figure S5). Except for a slight birefringence change, the mosaic texture keeps quite unaltered even on further cooling below the transition at 81 °C (Fig. S5). On the other hand, the enthalpy associated to this transition is very small (Table 1) and leads to small changes in the mesophase organization. It should be also noted that, on cooling below 153 °C an increase in the viscosity of the sample could be clearly observed by pressing the thin LC film over the cover glass slide. This indicates that the SmX1/SmX2 transition (Table 1) leads to a highly ordered smectic phase, in agreement to its relatively large  $\Delta H$  value. The compound **8.3bp8** shows similar POM textures (Figure 1c and Figure S8 in ESI) to those of **8.2bp7**, but it exhibits a higher clearing point and a lower crystallization temperature, leading to an extended range of existence of the mesophase down to about 57 °C. Therefore, increasing the alkyl chain and the alkyl spacer length of 1 carbon atom we get a wider mesophase range due to lower melting as well as higher clearing point.

**8.2bp12** shows a more interesting behaviour since it exhibits also a SmA phase. This can be clearly identified by the appearance of bâtonnets on cooling from the isotropic phase (Figure S10), which evolve to the typical fan-shaped texture (Figure 1d). It is noteworthy that the clearing point was clearly visible under the microscope both on heating and on cooling, but the transition was not sharp. Similarly, the identification of the Iso-SmA transition in the DSC trace was not easy (Figure S9). The thermotropic behaviour of compound **8.2bp14**, is illustrated in Figure S12 of ESI. On cooling from the Isotropic phase (5 °C/min) (just below 230 °C), bâtonnets are observed under POM which, upon aggregation, evolve into a fan-like texture, typical of a SmA phase (Figure S12a) ESI). Another transition can be clearly detected at 180 °C leading to a new mesophase characterized by a mosaic texture (Figure S12b) ESI). On further cooling below 56 °C a striated texture occurs which is indicative of the formation of a glassy mesophase (Figure S12c).

**10.2bp14** and **10.2bp16** are obtained by further extending the length of both diverse moieties; they show a similar thermal behaviour: both exhibit a SmA phase, as suggested by the batonnet textures and focal conic textures observed on cooling from the melt at relatively high temperature (see Figure 1e and Figures S14 and S16 of ESI).

Regarding the Oxadiazole-extended viologens series **Lobpl**, all of them show clearing temperatures higher than 150 °C and show ordered mesophases. Within the symmetric non polyfluorinated series **Lobpl**, **10obp10** shows smectic bâtonnets on cooling from the isotropic state that evolve into a fan shaped texture down to about 120 °C (Figure S18a), where another transition is detected in the thermogram (Fig. S17). Below this temperature, the LC film becomes less soft and striation across the fan can be observed on the texture (Figures 1f and S18b), indicating the occurrence of a transition to a more ordered smectic phase.

**Table 1.** Thermal data obtained during the cooling run of the bistriflimide compounds studied. Onset transition temperatures in °C and enthalpy of transition in kJ/mol.

Compound	T (°C)	$\Delta H$ (kJ/mol)	Transition
<b>1.2bp14</b>	63 <sup>a</sup>	n.d.	Iso – SmX <sup>c</sup>
	44.8	13.5	SmX – Cr
<b>6.2bp8</b>	158.7	5.1	Iso – SmX
	49.3	13.2	SmX – Cr
<b>8.2bp7</b>	190 <sup>a</sup>	nd	Iso – SmX1
	155.1	3.7	SmX1 – SmX2
	80.7	0.1	SmX2 – Cr
<b>8.3bp8</b>	202.7	9.8	Iso – SmX
	57.2	3.0	SmX – Cr
<b>8.2bp12</b>	228 <sup>a</sup>	ca. 1 <sup>b</sup>	Iso – SmA
	199.8	1.3	SmA – SmX1
	139.4	0.9	SmX1 – SmX2
	106.9	2.1	SmX – Cr
<b>8.2bp14</b>	236.4	3.9	Iso – SmA
	169.5	2.2	SmA – SmX
	54.7	5.6	SmX – Cr
<b>10.2bp14</b>	220.4	0.4	Iso – SmA
	190.5	4.5	SmA – SmX
	126.3	5.8	SmX – Cr
<b>10.2bp16</b>	255.3	0.2	Iso – SmA
	189.6	2.8	SmA – SmX
	126.1	12.2	SmA – Cr
<b>10obp10</b>	170 <sup>a</sup>	nd	Iso – SmA
	119.6	5.0	SmA – SmX
	34.7	1.8	SmX – Cr
<b>12obp12</b>	151.1	4.9	Iso – B <sub>n</sub> <sup>d</sup>
	77.3	1.0	B <sub>n</sub> – Cr
<b>14obp14</b>	208 <sup>a</sup>	nd	Iso – B <sub>n</sub>
	173.5	7.5	B <sub>n</sub> – B <sub>m</sub> <sup>d</sup>
	71.5	8.5	B <sub>m</sub> – Cr
<b>8.2obp2.8</b>	250		Decomp.

<sup>a</sup>From POM observation on cooling from the Iso state; <sup>b</sup>estimated from the very broad DSC heating trace (Fig. S9); nd = not detected in DSC. <sup>c</sup>Unidentified smectic phase; <sup>d</sup>unidentified banana phase

By increasing the length of the alkyl chains, we observe the formation of dendritic textures for **12obp12** (Figure 1g and Figure S20) and **14obp14** (Figure 1h and Figure S22), which recall the behaviour of banana phases. In particular, the POM analysis of **12obp12** clearly evidences the formation of dendritic aggregates and lancets with jagged edges on cooling from the Iso state (Fig. S20 a and b). This texture is maintained down to room temperature but, below 78 °C, striations across the

dendritic domains can be clearly observed together with the formation of longitudinal isotropic domains along the lancets, which recall the shape of spear arrows (Figures 1g and S20c). This transformation indicates the transition to a crystal phase, according to the DSC analysis (Figure S19).

An analogous behaviour has been observed for the compound **14obp14** (Figure S22a) but, the dendritic aggregates transform into a mosaic texture (Figure S22b) on cooling below the transition found in the thermogram at 173 °C. Upon further cooling below the transition at 71 °C, another significant change of texture occurs that can be associated to the formation of a crystal phase (Figure S22c).

Even though the behaviour of these samples is usually found in banana phases, a definitive assignment of the type of mesophase requires further investigation.

Based on the DSC analysis and POM micrographs we illustrate the sequence of phases of the investigated salts and their thermal range of stability by histogram bars in Figure 2.

A quite general trend that can be traced up by taking into account Figure 2, is that the clearing temperature generally decreases with the reduced symmetry of the viologen substitution, both in terms of different length and type (alkyl/polyfluoroalkyl) of the chains, and with the overall decrease of the chain length, in agreement with the behaviour of non-symmetric alkylviologens **MbpL** (M=3-8, L=8-11).<sup>5</sup> In particular, this trend is as effective as to give rise to the ionic liquid **1.2bp14**. Some systematic behaviour can also be observed within the series **M.2bp14**, having the same alkyl chain but different length of the fluorinated chain. In this case, a less symmetric substitution leads to a mesophase stabilization at lower temperature.

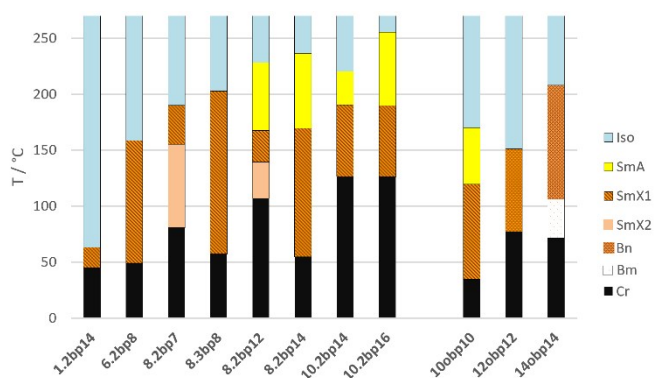


Figure 2. Thermal behaviour and range of stability of the investigated bistriflimide salts.

On the other hand, if we consider the series **8.2bpL**, where an asymmetry inversion occurs, there is a tendency of the clearing temperature to increase with the increase of the alkyl chain length. In this homologous series, the asymmetry inversion leads to the formation of a high temperature SmA phase which is also found in the **10.2bpL** series, in contrast to alkylated viologens bistriflimide with comparable chain lengths, e.g. **14bp14**, for which only ordered smectic phases were observed.<sup>3</sup> Thus, it appears that polyfluorinated systems can exhibit a SmA

phase even with a shorter chain when compared with alkylated systems. This result was already reported for imidazolium salts.

In fact, it is well-known that the existence of a SmA phase is related to the alkyl chain length and, for example, for alkyl-methylimidazolium iodide salts, a SmA phase can be found only for alkyl chains with at least 11 carbon atoms.<sup>57</sup> However, polyfluorinated imidazolium salts exhibit a SmA phase even with shorter chains, e.g. a polyfluorinated methylimidazolium where the carbon chain is of just 8 carbon atoms.<sup>55</sup>

Also, triazolium bistriflimide salts containing both perfluoroalkyl and alkyl chains exhibit SmA mesophase with C7 perfluorinated chains and C10 alkyl chain.<sup>56</sup> No investigation for shorter alkyl chain is reported to assess the minimum alkyl chain length necessary for mesophase aggregation. Interestingly the same cationic scaffold with C10 alkyl chain and a shorter perfluorinated chain (namely C<sub>3</sub>F<sub>7</sub>), being the anion the same bistriflimide, did not show any mesophase.<sup>56</sup>

### Cyclic Voltammetry (CV)

All viologens display two irreversible cathodic waves, in the range -0.2 – -1.0 V (all potentials vs. Ag/AgCl), ascribable to two mono electronic redox transitions (Figure S23 and Table S1). On the other hand, upon scanning only until -0.65 V, the first reduction waves become quasi-reversible (Figure S24). For all samples of the **M.2bpL** series, this can be observed at  $E_{1/2} = -0.32$  –  $-0.32$  V (with  $\Delta E (E_{pc} - E_{pa}) = 77$ -101 mV), being basically unaffected by the alkyl chains length. A shift is instead observed for **8.3bp8**, which is more difficult to reduce ( $E_{1/2} = -0.35$  V,  $\Delta E = 79$  mV), owing to the longer alkyl spacer conjugating the heterocycle and the electron withdrawing perfluoroalkyl residue. With respect to the non-fluorinated viologen **8bp8** ( $E_{1/2} = -0.39$  V,  $\Delta E = 78$  mV), a fluorinated chain with a C3 spacer makes the reduction easier by ca. 40 mV (for **8.3bp8**). A shorter (C2) spacer has a stronger effect (reduction easier by ca. 80 mV for **10.2bp16**), while increasing the fluorinated chain (for example, going from **1.2bp14**, to **10.2bp16** has only a small effect (ca. 8 mV).

For the oxadiazolylbipyridinium compounds, the first reduction steps require a more negative potential ( $E_{1/2} = -0.43$  V,  $\Delta E = 82$ -100 mV), with the exception of **8.2obp2.8** ( $E_{1/2} = -0.37$  V,  $\Delta E = 84$  mV), for which the presence of the fluorinated chain anticipates by ca. 60 mV the reduction with respect to fluorine-free samples (Figure S25 and Table S1). The second reduction step is much easier for **8.2obp2.8** ( $E_{1/2}$  at -0.75 V, being anticipated by 40 mV with respect to **10obp10** ( $E_{1/2} = -0.71$  V, Figure S26). The voltammetric trace is, however, much less defined for the fluorinated sample, for which both reductions are strongly irreversible.

These experimental results can be compared with the prediction of DFT calculations. To reduce the computational complexity, we selected model systems with relatively short chains. We do not intend to quantitatively predict the electrochemical properties, rather to assess whether the inductive effect of the polyfluoro chain is responsible of the observed shifts. To this end, following Ref.<sup>58</sup>, we have calculated the electronic energy (B3LYP/6-311+G(d,p), PCM solvation

model of acetonitrile) of the singlet dication and the doublet radical monocation; the energy difference is an estimation of the electron affinity of the dication molecule. We use the following model systems:  $\text{CF}_3\text{-CH}_2\text{-bp-CH}_2\text{-CH}_3$  as a model of polyfluorinated viologens (**1.1bp2**, following the labeling used for the experimental systems);  $\text{CH}_3\text{-CH}_2\text{-bp-CH}_2\text{-CH}_3$  as a model of a simple viologen (**2bp2**); and  $\text{CH}_3\text{-obp-CH}_3$  as a model of the oxadiazolyl bipyridinium systems (**1obp1**).

The calculated  $\Delta E$ (dication-radical monocation) are shown in Table 2 and are well correlated, at least qualitatively, with the reduction potentials  $E_{1/2}$ : an increased calculated electron affinity corresponds to an easier reduction. In contrast, there is no correlation, even at a qualitative level, with the HOMO-LUMO gap (see ESI), indicating that when comparing different systems, the HOMO-LUMO gap is not a reliable indicator of the easiness of reduction.

**Table 2.** Experimental reduction potential,  $E_{1/2}$ , (vs. Ag/AgCl) and DFT data relative to the model pairs singlet dication/doublet monocation.

	$\Delta E$ (eV)	$E_{1/2}$ (V)	$E_{\text{LUMO}}^d$	$E_{\text{HOMO}}^d$	$\Delta E(\text{H-L})$
<b>1.1bp2</b>	4.460	-0.32 <sup>a</sup>	-0.14902	-0.33545	0.18643
<b>2bp2</b>	4.264	-0.38 <sup>b</sup>	-0.14223	-0.33343	0.19120
<b>1obp1</b>	4.155	-0.43 <sup>c</sup>	-0.14343	-0.31929	0.17586

<sup>a</sup>compound **1.2bp14**; <sup>b</sup>compound **8bp8**; <sup>c</sup>compound **10obp10**; <sup>d</sup>HOMO and LUMO of dicationic singlet species.

### Spectroelectrochemistry in Solution.

Vis-NIR (350-1400 nm) spectroelectrochemical characterization was performed in acetonitrile solution. The electrochromic response of the **M.2bpL<sup>++</sup>** dicationic systems is analogous to that of the classic viologen,<sup>59,60</sup> with two absorptions at ~400 nm and ~600 nm that grow simultaneously when monoreduction begins at about -0.2 V vs. AgCl/Ag and reach the maximum intensity in correspondence to the first half wave reduction peak observed in the CVs (Figure 3a and Figure S27). These absorption bands characterize the viologen radical cation (**M.2bpL<sup>•+</sup>**) which is blue colored. Bleaching occurs at higher negative potentials due to the formation of the neutral species (Figure 3b). The spectroelectrochemical data do not show any clear dependence of the electrochromic response on the structure of the compounds within the series studied. However, they suggest that the length of the polyfluorinated chain affects the molar extinction coefficient ( $\epsilon$ ) which is the highest for the compounds **8.2bpL** (Figure 3).

In contrast to the classic bipyridinium systems, the spectroelectrochemical study performed on the oxadiazolyl derivatives **10obp10**, **14obp14** and **8.2obp2.8** shows that they are not electrochromic on reduction to the radical cation species (Figure S27) despite they do form this species (see CV in Figures S25 and S26 in ESI). The lack of the typical absorption band of the radical cation is due to a failure of the optically induced intervalence charge transfer mechanism between the nitrogen atom with formally zero charge and that with formally +1 charge,<sup>61,62</sup> which occurs only when the two redox centers are electronically coupled as in mixed valence systems of Robin and Day class II and III.<sup>63,64</sup> Therefore, the oxadiazolyl insertion hampers the resonance communication between the redox

centers of the pyridinium moieties, as expected, in contrast to what observed on other "extended viologens".<sup>10,37,39,42,61,69-71</sup> This conclusion is also supported by DFT calculations (B3LYP/6-311+G(d,p) level of theory) showing that the electron configuration of the radical cations of the two series of viologens are very different. In the classic viologens, the electron spin density of the doublet radical monocation is distributed on both the bipyridinium rings (Fig. 4a), which is reflected also in a rather homogeneous distribution of the positive charge across the whole cation (see the electrostatic potential map in ESI), indicating a resonance coupling between the two redox centers. In contrast, in the oxadiazolylviologens, the electron spin density is localized on one ring (Fig. 4b) and the electrostatic potential map shows that the positive charges is mainly concentrated on one side of the extended viologen core (Fig. S29-S31).

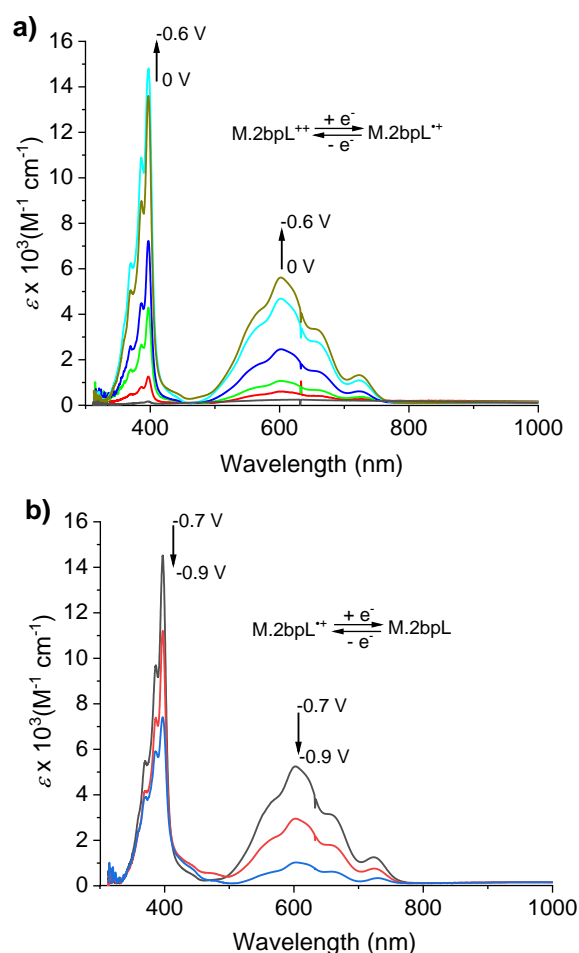


**Figure 3.** Vis-NIR spectroelectrochemistry of the compound **8.2bp14** as representative of that of the **M.2bp.L** series. Arrows indicate band growth a) and band bleaching b) with increasing negative potential. The potentials are referenced to AgCl/Ag. The reactions in the insets show the formation of the radical cation a) and the neutral species b) at the working electrode.

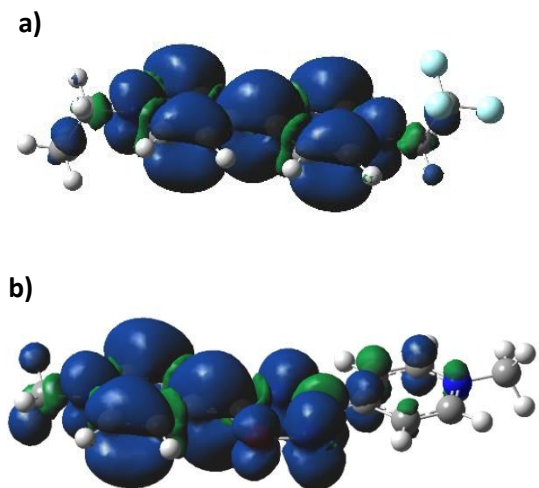


**Figure 4.** Electron spin density of the radical cations of a) polyfluoroalkylviologens [CF<sub>3</sub>CH<sub>2</sub>bpCH<sub>2</sub>CH<sub>3</sub>]<sup>•+</sup> (**1.2bp2**) and b) oxadiazolylviologens [CH<sub>3</sub>obpCH<sub>3</sub>]<sup>•+</sup> (**1obp1**)

#### Bulk Spectroelectrochemistry of viologens.

Bulk spectroelectrochemical characterization was performed on some of the viologens reported in Table 1 by considering those forming stable mesophases close to room temperature.

The liquid crystal **8.2bp14** exhibits electrochromism in the bulk when a thin LC film (5 μm) is sandwiched between two ITO glass substrates. The EC response is observable above about 2.5 V at 214 °C in the smectic phase (see Figure S28). However, the intensity of the electrochromic bands is very low (Figure S28). Due to the high temperature needed to achieve the mesophases and the low EC response, we did not further investigate such compound.

More interesting results were gained by the study of the bulk electrochromism of the LC compound **1.2bp14**, which has a very low clearing temperature (63 °C) and forms a mesophase with a marble like texture on cooling from the Iso state (Figure 1). Figure 5 shows the spectroelectrochemistry of a thin film (5 μm)

of **1.2bp14** in the LC state at 52 °C. The liquid crystalline cell was assembled by sandwiching the material between a ITO electrode on one side and a TiO<sub>2</sub>-coated ITO electrode on the other side. It can be seen the close similarity between the bulk electrochromic response of the viologen in the Vis range with that occurring in solution (Figure 3). Indeed, the two bands at 400 nm and 600 nm, typical of the viologen monocation radical, are found also in the LC state, with the latter shifted to lower wavelengths. However, the bulk spectrum of the radical cation shows also an absorption band in the NIR range, centered at 860 nm). A similar behaviour was already observed with the methylviologen chloride in water and has been attributed to a radical cation dimerization.<sup>59,68</sup> More recently, it was also observed in thin films of viologens-based cyclophanes.<sup>69</sup> The formation of the dimer in the mesophase should be largely favoured by the close proximity in which the radical cations are organized in the smectic phase.

All the above bands grow in intensity as the potential difference applied to the LC cell is increased. The above spectral changes cause a colour switching of the LC film from colourless (0 V) to violet. This can be seen in the Video S1, showing the LC cell placed on the hot plate of the Linkam at 52 °C during the application of the potential switching. The electric voltage was biased between the two ITO electrodes by an external potentiostat, at 4V, through the Linkam internal contacts. Video S1 clearly shows a reversible electrochromic response, characterized by a very fast coloration kinetics (a fraction of a second) and a slower (a few seconds) bleaching. The same experimental set-up described above was used to visualize the electrochromic response under POM. Video S2 shows the change of the LC texture upon switching from 0 V to increasing potential bias up to 4 V (Figure 5b). The LC film texture becomes gradually darker as the voltage is increased and bleaches as the voltage bias is removed. Notably, it is worth to highlight the stability of the mesophase texture during the reduction process, indicating that the electrochromic mechanism involves the injection of the electronic charges from the ITO electrodes into the LC film and their transport through the film by hopping between reduced and oxidized viologen species, which does not affect the mesophase organization.<sup>70</sup>

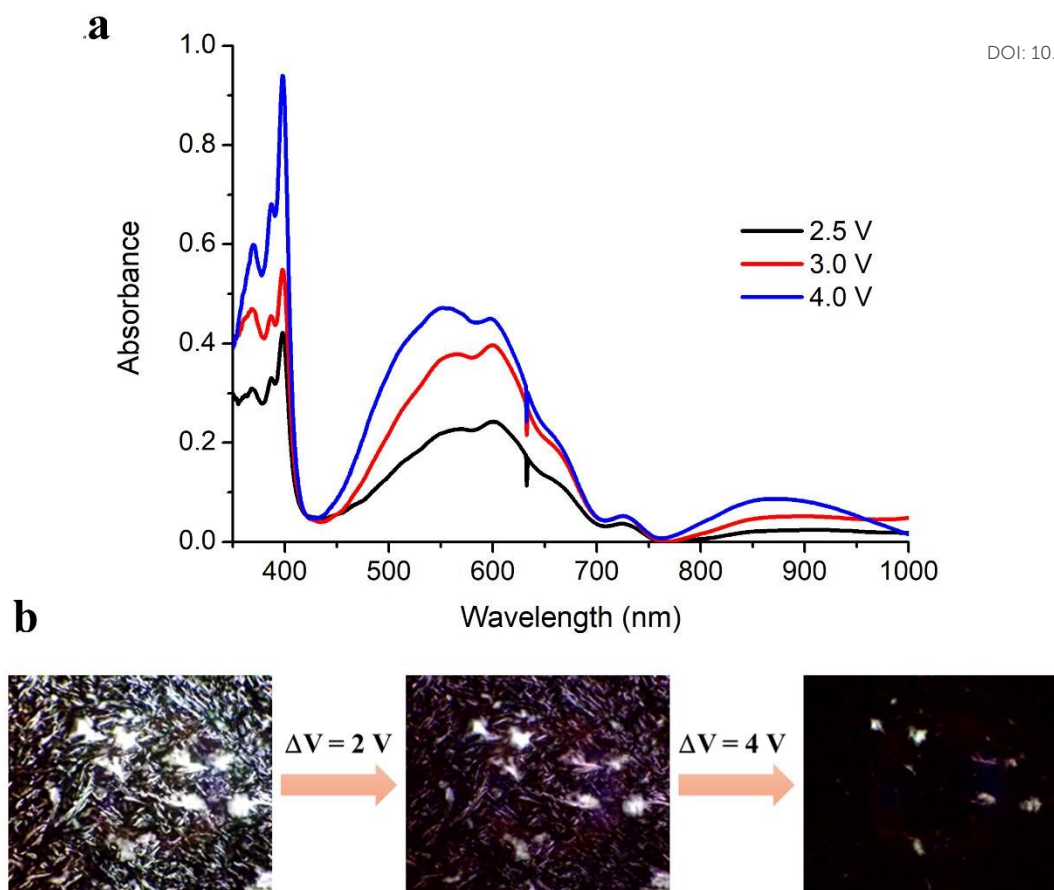


**Figure 5.** a) Bulk spectroelectrochemistry of **1.2bp14** at 52 °C. b) POM images of a thin film (5  $\mu\text{m}$ ) of **1.2bp14** sandwiched in a ITO/TiO<sub>2</sub>-ITO liquid crystalline cell, acquired during the reduction process as a function of the applied voltage difference.

## Conclusions

In summary, we prepared two different classes of bistriflimide salts based on bipyridinium scaffolds: viologens asymmetrically substituted with hydro/fluorocarbon chains of different length and symmetrically substituted bipyridinium in which the two pyridinium moieties are separated by an oxadiazole spacer, conferring a bent shape to the molecule and interrupting the conjugation. The thermal and spectroelectrochemical behaviour of these salts has been explored allowing us to observe in almost all the cases the formation of thermotropic and enantiotropic mesophases. Both alkyl and perfluoroalkyl chain lengths are able to influence the molecular micro-segregation, improving the mesophase range and stability. On the other hand, the oxadiazole spacer confers special mode of aggregation to these systems, leading to dendritic textures characteristic of banana phases.

The electrochemical stability of these ionic liquid crystals has been assessed by cyclic voltammetry and their spectroelectrochemical properties were investigated in solution and, in some cases, in the liquid crystalline phase. It has been observed that the compounds of the viologen series exhibit an electrochromic response typical of the classic alkyl viologens in solution. In contrast, those of the oxadiazolylbipyridinium series did not show any electrochromism. The cause of the latter behaviour has been addressed to the fact that the bent core, and the peculiar electronic structure, does not allow the electron communication between the pyridine units.

The electrochromic behaviour of the viologen series has been further investigated in the bulk LC phase. Upon reduction to the radical cation species, the LC film showed a very rapid colour switch from colourless to violet. Notably, the electrochromic response was rather unusual compared to that observed in solution because, the spectroelectrochemical investigation showed the appearance of a new electrochromic band in the near infrared range which has been associated to a radical cation dimerization.

This report represents a significant step in the rationalization of the thermal behaviour and of the physical and electrochemical properties of ionic materials based on hydro/fluoro-carburic bipyridinium salts. The studied systems allowed to consider the effect of several structural and chemical features of the constituent molecules and their impact on the macroscopic properties of the materials.

## Conflicts of interest

There are no conflicts to declare.

## Acknowledgements

Calculations were run on the Linux cluster "Avogadro" of the C3p community of the Department of Chemical Sciences of the

University of Padova. We thank the bilateral agreement CNR-CAS 2017-2019 and the University of Palermo PJ\_RIC\_FFABR\_2017\_160324 for financial support.

## Notes and references

- H. Tahara, Y. Furue, C. Suenaga and T. Sagara, *Cryst. Growth Des.*, 2015, **15**, 4735–4740.
- G. Casella, V. Causin, F. Rastrelli and G. Saielli, *Liq. Cryst.*, 2016, **43**, 1161–1173.
- G. Casella, V. Causin, F. Rastrelli and G. Saielli, *Phys. Chem. Chem. Phys.*, 2014, **16**, 5048–5051.
- M. Bonchio, M. Carraro, G. Casella, V. Causin, F. Rastrelli and G. Saielli, *Phys. Chem. Chem. Phys.*, 2012, **14**, 2710–2717.
- V. Causin and G. Saielli, *J. Mater. Chem.*, 2009, **19**, 9153–9162.
- P. K. Bhowmik, H. S. Han, J. J. Cebe, R. A. Burchett, B. Acharya and S. Kumar, *Liq. Cryst.*, 2003, **30**, 1433–1440.
- S. Asaftei, M. Ciobanu, A. M. Lepadatu, S. Enfeng and U. Beginn, *J. Mater. Chem.*, 2012, **22**, 14426–14437.
- W. Sliwa and B. B. and T. Girek, *Curr. Org. Chem.*, 2012, **16**, 1332–1358.
- A. Liu, H. Che and R. Jiang, *J. Porous Mater.*, 2013, **20**, 579–586.
- M. Ciobanu and S. Asaftei, *Opt. Mater. (Amst.)*, 2015, **42**, 262–269.
- C. R. Rigby, H. Han, P. K. Bhowmik, M. Bahari, A. Chang, J. N. Harb, R. S. Lewis and G. D. Watt, *J. Electroanal. Chem.*, 2018, **823**, 416–421.
- N. Jordão, L. Cabrita, F. Pina and L. C. Branco, *Chem. Eur. J.*, 2014, **20**, 3982–3988.
- N. Jordão, H. Cruz, A. Branco, F. Pina and L. C. Branco, *Chempluschem*, 2015, **80**, 202–208.
- N. Jordao, H. Cruz, A. Branco, C. Pinheiro, F. Pina and L. C. Branco, *RSC Adv.*, 2015, **5**, 27867–27873.
- R. P. Singh and J. M. Shreeve, *Inorg. Chem.*, 2003, **42**, 7416–7421.
- R. Shi and Y. Wang, *Sci. Rep.*, 2016, **6**, 19612–19644.
- K. Goossens, K. Lava, C. W. Bielawski and K. Binnemans, *Chem. Rev.*, 2016, **116**, 4643–4807.
- P. K. Bhowmik, H. S. Han, I. K. Nedeltchev and J. J. Cebe, *Mol. Cryst. Liq. Cryst.*, 2004, **419**, 27–46.
- P. K. Bhowmik, H. S. Han, S. Akhter and H. S. Han, *J. Polym. Sci. Part a-Polymer Chem.*, 1995, **33**, 1745–1749.
- P. K. Bhowmik, W. H. Xu and H. S. Han, *J. Polym. Sci. Part a-Polymer Chem.*, 1994, **32**, 3205–3209.
- P. K. Bhowmik, S. T. Killarney, J. R. A. Li, J. J. Koh, H. Han, L. Sharpnack, D. M. Agra-Kooijman, M. R. Fisch and S. Kumar, *Liq. Cryst.*, 2018, **45**, 872–885.
- V. Causin and G. Saielli, *J. Mol. Liq.*, 2009, **145**, 41–47.
- T. Kobayashi and T. Ichikawa, *Materials (Basel)*, 2017, **10**, 1243.
- K. Tanabe, T. Yasuda, M. Yoshio and T. Kato, *Org. Lett.*, 2007, **9**, 4271–4274.
- T. Li, F. Xu and W. Shi, *Chem. Phys. Lett.*, 2015, **628**, 9–15.
- R.-T. Wang, G.-H. Lee and C. K. Lai, *J. Mater. Chem. C*, 2018, **6**, 9430–9444.
- A. Beneduci, S. Cospito, A. Crispini, B. Gabriele, F. P. Nicoletta, L. Veltri and G. Chidichimo, *J. Mater. Chem. C*, 2013, **1**, 2233–2240.
- L. Veltri, V. Maltese, F. Auriemma, C. Santillo, S. Cospito, M. La Deda, G. Chidichimo, B. Gabriele, C. De Rosa and A. Beneduci, *Cryst. Growth Des.*, 2016, **16**, 5646–5656.
- S. Cospito, A. Beneduci, L. Veltri, M. Salamonczyk and G. Chidichimo, *Phys. Chem. Chem. Phys.*, 2015, **17**, 17670–17678.
- A. Beneduci, S. Cospito, M. La Deda, L. Veltri and G. Chidichimo, *Nat. Commun.*, 2014, **5**, 3105.
- A. Beneduci, S. Cospito, M. La Deda and G. Chidichimo, *Adv. Funct. Mater.*, 2015, **25**, 1240–1247.
- A. Beneduci, S. Cospito, D. Imbardelli, B. C. De Simone and G. Chidichimo, *Mol. Cryst. Liq. Cryst.*, 2015, **610**, 108–115.
- A. Pace, S. Buscemi, A. P. Piccionello and I. Pibiri, eds. E. F. V Scriven and C. A. Ramsden, Academic Press, 2015, vol. 116, pp. 85–136.
- I. Pibiri, A. Pace, S. Buscemi, V. Causin, F. Rastrelli and G. Saielli, *Phys. Chem. Chem. Phys.*, 2012, **14**, 14306–14314.
- M. Saccone, G. Cavallo, P. Metrangolo, A. Pace, I. Pibiri, T. Pilati, G. Resnati and G. Terraneo, *CrystEngComm*, 2013, **15**, 3102–3105.
- A. Maio, D. Giallombardo, R. Scaffaro, A. Palumbo Piccionello and I. Pibiri, *RSC Adv.*, 2016, **6**, 46037–46047.
- A. P. Piccionello, A. Calabrese, I. Pibiri, V. Giacalone, A. Pace and S. Buscemi, *J. Heterocycl. Chem.*, 2016, **53**, 1935–1940.
- A. Maio, R. Scaffaro, L. Lentini, A. Palumbo Piccionello and I. Pibiri, *Chem. Eng. J.*, 2018, **334**, 54–65.
- F. S. Palumbo, M. Di Stefano, A. Palumbo Piccionello, C. Fiorica, G. Pitarresi, I. Pibiri, S. Buscemi and G. Giammona, *RSC Adv.*, 2014, **4**, 22894–22901.
- F. Lo Celso, I. Pibiri, A. Triolo, R. Triolo, A. Pace, S. Buscemi and N. Vivona, *J. Mater. Chem.*, 2007, **17**, 1201–1208.
- L. Lentini, R. Melfi, A. Di Leonardo, A. Spinello, G. Barone, A. Pace, A. Palumbo Piccionello and I. Pibiri, *Mol. Pharm.*, 2014, **11**, 653–664.
- I. Pibiri, L. Lentini, R. Melfi, G. Gallucci, A. Pace, A. Spinello, G. Barone and A. Di Leonardo, *Eur. J. Med. Chem.*, 2015, **101**, 236–244.
- I. Pibiri, L. Lentini, M. Tutone, R. Melfi, A. Pace and A. Di Leonardo, *Eur. J. Med. Chem.*, 2016, **122**, 429–435.
- S. Rubino, I. Pibiri, C. Costantino, S. Buscemi, M. A. Girasolo, A. Attanzio and L. Tesoriere, *J. Inorg. Biochem.*, 2016, **155**, 92–100.
- S. Rubino, I. Pibiri, C. Minacori, R. Alduina, V. Di Stefano, S. Orecchio, S. Buscemi, M. A. Girasolo, L. Tesoriere and A. Attanzio, *Inorganica Chim. Acta*, 2018, **483**, 180–190.
- I. Pibiri, L. Lentini, R. Melfi, M. Tutone, S. Baldassano, P. Ricco Galluzzo, A. Di Leonardo and A. Pace, *Eur. J. Med. Chem.*, 2018, **159**, 126–142.
- M. Tutone, I. Pibiri, L. Lentini, A. Pace and A. M. Almerico, *ACS Med. Chem. Lett.*, 2019, **10**, 522–527.
- H. Gallardo, R. Cristiano, A. A. Vieira, R. A. W. Neves Filho, R. M. Srivastava and I. H. Bechtold, *Liq. Cryst.*, 2008, **35**, 9430–9444.

View Article Online

DOI: 10.1039/C9TC01697J

- 857–863.
- 49 M. L. Parra, P. I. Hidalgo, E. A. Soto-Bustamante, J. Barberá, E. Y. Elgueta and V. H. Trujillo-Rojo, *Liq. Cryst.*, 2008, **35**, 1251–1262.
- 50 M. L. Parra, P. I. Hidalgo and E. Y. Elgueta, *Liq. Cryst.*, 2008, **35**, 823–832.
- 51 O. Francescangeli, V. Stanic, S. I. Torgova, A. Strigazzi, N. Scaramuzza, C. Ferrero, I. P. Dolbnya, T. M. Weiss, R. Berardi, L. Muccioli, S. Orlandi and C. Zannoni, *Adv. Funct. Mater.*, 2009, **19**, 2592–2600.
- 52 G. Shanker, M. Prehm and C. Tschierske, *Beilstein J. Org. Chem.*, 2012, **8**, 472–485.
- 53 I. Pibiri, A. Pace, S. Buscemi, N. Vivona and L. Malpezzi, *Heterocycles*, 2006, **68**, 307–321.
- 54 I. Pibiri, A. Pace, A. P. Piccionello, P. Pierro and S. Buscemi, *Heterocycles*, 2006, **68**, 2653–2661.
- 55 A. Abate, A. Petrozza, G. Cavallo, G. Lanzani, F. Matteucci, D. W. Bruce, N. Houbenov, P. Metrangolo and G. Resnati, *J. Mater. Chem. A*, 2013, **1**, 6572–6578.
- 56 A. Riccobono, R. R. Parker, A. C. Whitwood, J. M. Slattery, D. W. Bruce, I. Pibiri and A. Pace, *Chem. Commun.*, 2018, **54**, 9965–9968.
- 57 C. J. Bowlas, D. W. Bruce and K. R. Seddon, *Chem. Commun.*, 1996, 1625–1626.
- 58 C. Boga, M. Calvaresi, P. Franchi, M. Lucarini, S. Fazzini, D. Spinelli and D. Tonelli, *Org. Biomol. Chem.*, 2012, **10**, 7986–7995.
- 59 Monk, *The Viologens, physicochemical properties, synthesis and applications of the salts of 4,4'-bipyridine*, John Wiley & Sons, Ltd, 1998, pp. 55–64.
- 60 G. Chidichimo, B. C. De Simone, D. Imbardelli, M. De Benedittis, M. Barberio, L. Ricciardi and A. Beneduci, *J. Phys. Chem. C*, 2014, **118**, 13484–13492.
- 61 K. Takahashi, T. Nihira, K. Akiyama, Y. Ikegami and E. Fukuyo, *J. Chem. Soc. Chem. Commun.*, 1992, 620–622.
- 62 W. W. Porter, T. P. Vaid and A. L. Rheingold, *J. Am. Chem. Soc.*, 2005, **127**, 16559–16566.
- 63 G. A. Corrente, E. Fabiano, F. Manni, G. Chidichimo, G. Gigli, A. Beneduci and A.-L. Capodilupo, *Chem. Mater.*, 2018, **30**, 5610–5620.
- 64 A. Beneduci, G. A. Corrente, E. Fabiano, V. Maltese, S. Cospito, G. Ciccarella, G. Chidichimo, G. Gigli and A.-L. Capodilupo, *Chem. Commun.*, 2017, **53**, 8960–8963.
- 65 W. M. Albers, G. W. Canters and J. Reedijk, *Tetrahedron*, 1995, **51**, 3895–3904.
- 66 A. N. Woodward, J. M. Kolesar, S. R. Hall, N.-A. Saleh, D. S. Jones and M. G. Walter, *J. Am. Chem. Soc.*, 2017, **139**, 8467–8473.
- 67 S. Cospito, B. C. De Simone, A. Beneduci, D. Imbardelli and G. Chidichimo, *Mater. Chem. Phys.*, 2013, **140**, 431–434.
- 68 E. M. Kosower and J. L. Cotter, *J. Am. Chem. Soc.*, 1964, **86**, 5524–5527.
- 69 K. Tanabe and T. Kato, *Chem. Commun.*, 2009, 1864–1866.
- 70 A. Beneduci, G. A. Corrente and G. Chidichimo, in *Electrochromic Smart Materials: Fabrication and Applications*, eds. J. W. Xu, M. H. Chua and K. W. Shah, The Royal Society of Chemistry, Cambridge, 2019, pp. 261–292.

View Article Online  
DOI: 10.1039/C9TC01697J

## Table of Contents Entry

View Article Online  
DOI: 10.1039/C9TC01697J



Non-symmetric alkyl/polyfluoroalkyl viologens with electrochromism in the smectic phase and mesomorphism of bent core oxadiazolyl viologens with hampered electrochromism